

Dendrite Morphological Analysis on SMA, GMA, and PGMA Welding of Dissimilar 304LN Austenitic Stainless Steel and Micro-alloyed Steel

G. Rajamurugan¹  · P. K. Ghosh² · K. Prabu¹ · D. Dinesh³ · S. M. Vinukumar³

Received: 28 January 2019 / Accepted: 17 January 2020 / Published online: 4 February 2020
© The Indian Institute of Metals - IIM 2020

Abstract Dissimilar metal welding between the austenitic stainless steel and micro-alloyed steel was widely used in high-temperature applications in power stations and petrochemical plants. In the current research, the dissimilar metals between austenitic stainless steel and micro-alloyed steel have been joined by shielded metal arc welding (SMA), gas metal arc welding (GMA), and pulse gas metal arc welding (PGMA) processes. Welded samples of the aforementioned processes were subjected to comparative studies pertaining to the dendrite morphological characteristics. The study reveals that the process parameters affect the growth of dendrite arm because of the variation in the coefficient of thermal conductivity, expansion, and metallurgical incompatibility of the metals. In the PGMA welding process, the dendrite length decreases, while its width increases in all the locations of the weld by varying dimensionless factors ϕ (0.05, 0.15, and 0.25) and keeping its heat input as constant (Ω —11.2 kJ/cm). Among the welded joints, the PGMA weld joint comparatively exhibit shorter length (20 μm) and width (4 μm) of dendrite arm than the welded joints of the GMA and SMA processes. The change in the dendrite dimension is observed to be due to the variation in the dimensionless factor ϕ and the

quantity of heat transfer to the weld (QT). The studies have been systematically planned in order to gain advanced scientific knowledge to establish superior technique for multi-pass PGMA welding of thick section of austenitic stainless steel to micro-alloy steel with respect to that used with conventional welding process.

Keywords Austenitic stainless steel · Micro-alloyed steel · Dendrite · Reheat refine region · Pulse current · Dissimilar welding

1 Introduction

Dissimilar metal welding (DMW) of thick-wall austenitic stainless steel (ASS) and high-strength low-alloy (HSLA) steel plates was used in the power generation, chemical, petrochemical, and nuclear industries where the temperature exceeded up to 400 °C [1]. Dissimilar weld joint was widely used in various industrial applications due to both technical and economic reasons [2]. The dissimilar metal welding (DMW) of thick section of ASS and micro-alloyed steel (MAS) was critical, and joining of carbon steel and stainless steel was challenging due to metallurgical mismatch, such as the formation of brittle phases, hydrogen cracks, solidification cracks [3–5], coefficient of thermal expansion (CTE) [6], distribution of residual stresses [7], and metallurgical incompatibility primarily with respect to the development of unwanted phases in the weld zone and HAZ [8]. The effect of the chemical discrepancy shows the separation of melting phases (high and low) [9]. These weld joints were subjected to repeated failures due to the formation of cracking at heat-affected zone (HAZ) during service in power plants caused by residual stresses.

✉ G. Rajamurugan
rajadmt@gmail.com

¹ School of Mechanical Engineering, Vellore Institute of Technology, Vellore, Tamilnadu 632014, India

² Department of Metallurgical and Materials Engineering, Indian Institute of Technology, Roorkee, Roorkee, Uttarakhand 247667, India

³ Department of Mechanical Engineering, Bannari Amman Institute of Technology, Sathyamangalam, Tamilnadu 638401, India

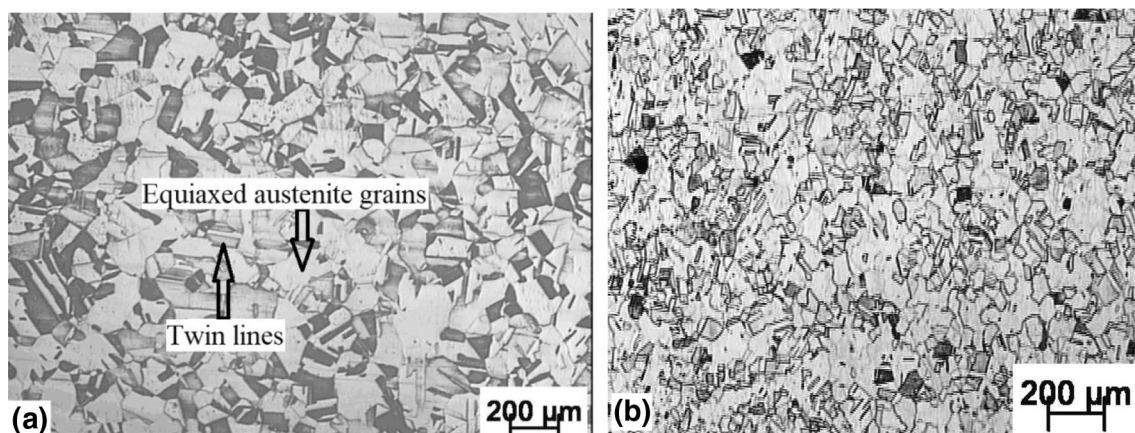


Fig. 1 Typical microstructure of the ASS base metal: **a** transverse direction and **b** longitudinal direction

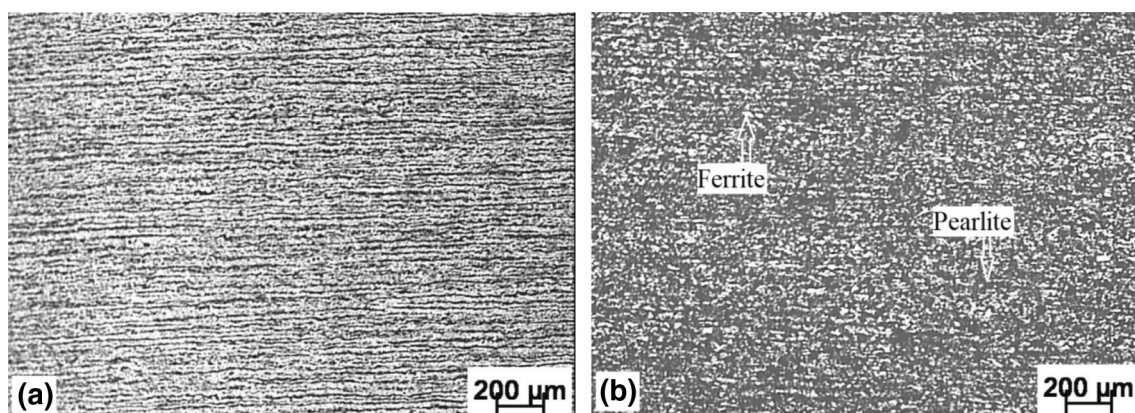


Fig. 2 Typical microstructure of the micro-alloyed steel base metal: **a** transverse direction and **b** longitudinal direction

Table 1 Chemical composition of base material and welding consumables

Material	Source	Chemical composition (wt%)									
		C	Cr	Ni	Mn	N	Mo	Si	Cu	S	P
ASS (304LN) Base metal	ASTM	0.035	18–20	8–11	2.0	0.1–0.16	–	0.75	–	0.03	0.04
	*	0.022	19.0	9.1	1.8	0.16	0.19	0.57	0.30	0.002	0.021
MAS SAILMA-410HI/SA543 Base metal	*	0.154	0.014	0.08 (v)	1.50	0.02 (Ti)	0.04 (Nb)	0.31	0.03	0.02	0.022
GTA welding electrode (ER308L)	*	0.021	18.8	11.7	2.0	–	0.20	0.40	0.08	0.01	0.019
SMA welding electrode (E308L-15)	*	0.046	18.7	11.9	1.8	–	0.1	0.22	0.12	0.006	0.016
GMAW filler wire (ER308L)	*	0.020	19.6	10.3	2.2	–	0.30	0.39	0.08	0.007	0.016

*Estimated chemical composition through spot emission spectroscopy

Fusion welding is the common welding process in the manufacturing industries for joining the dissimilar metals [10–15]. Each process has different welding parameters,

different weld thermal cycles, and a shielding environment. Among all of these fusion welding processes, GTAW and GMAW are attaining more consideration in fabrication of

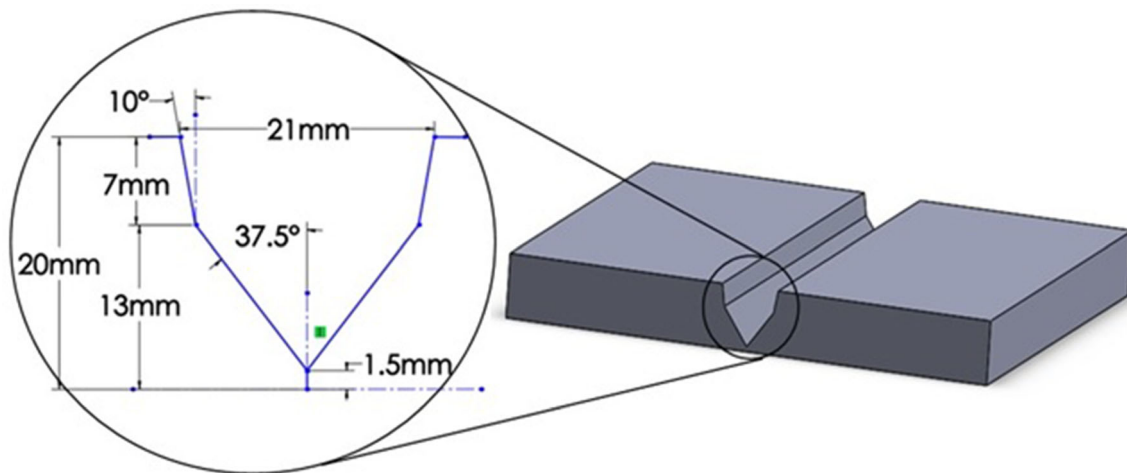


Fig. 3 Conventional V-groove for 21-mm-thick ASS and MAS steel plates

Fig. 4 Arrangement of welding fixture

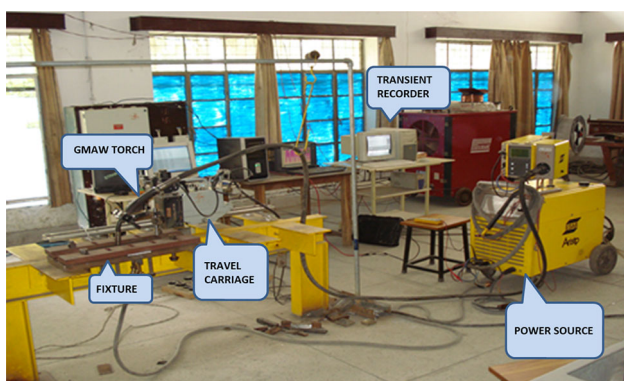
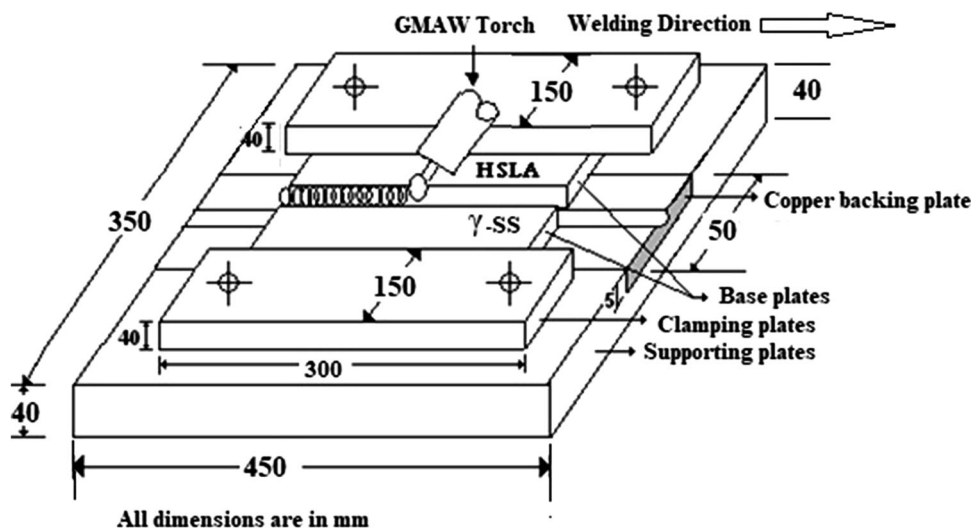
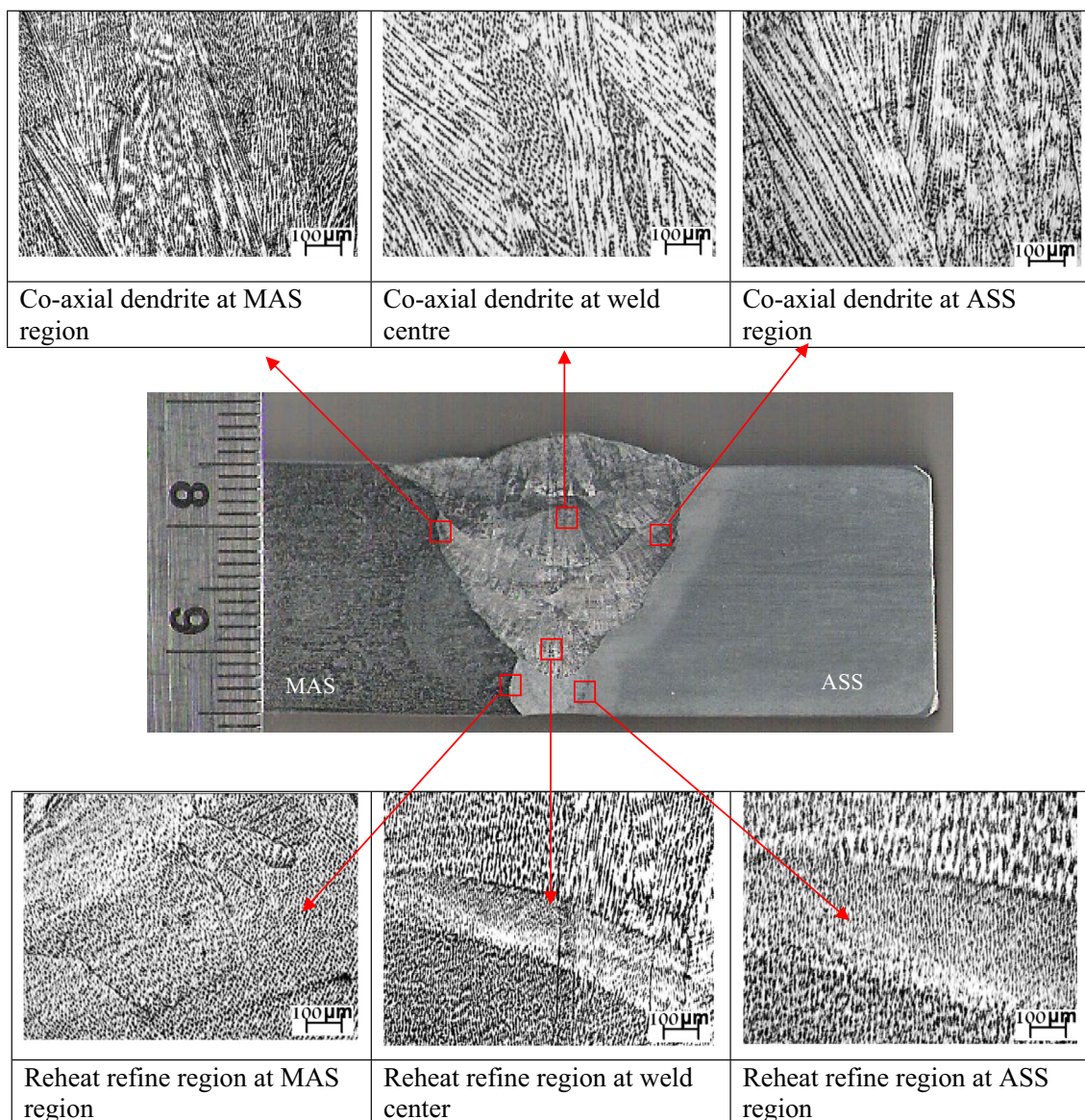


Fig. 5 Photograph of the experimental setup

dissimilar metal joint, due to their ability to develop better quality weldment, compared to manual metal arc welding (MMAW). However, as a comparatively low-heat input welding process, the GTAW is generally preferred for the root pass weld, but not for the filling passes in welding of thick sections [16]. The energy input is involved in a welding process, causing the melting of the filler and base metals also to develop certain reactions in a very short period of time, resulting in some dramatic changes in the HAZ microstructure adjacent to the fusion line. These changes primarily result from the rapid heating and cooling of the base materials during welding. The mechanical properties and grain structure are controlled by the weld

Table 2 Welding processes and their parameters

Ex. no.	Welding processes	Wire feed rate (m/min)	Heat input (kJ/cm)	ϕ	Travel speed S (cm/min)	Welding current I/I_m (A)	Arc voltage (V)	Pulse parameters				
								I_p (A)	I_b (A)	f (Hz)	t_p (ms)	t_b (ms)
1.	GTA	–	18-21	–	4-6	125-150	10 ± 2	–	–	–	–	–
2.	SMA	–	9-15	–	5-7	135-160	21 ± 3	–	–	–	–	–
3.	GMA	8.5-6.5	8-13	–	20	210 ± 3	24 ± 1	–	–	–	–	–
4.	PGMA	5.5	9.4	0.05–0.25	25	140-150	24 ± 1	435	33	100	2.7	7.3
		6	11.2			168-178	25.5 ± 1	440	34	120	2.7	5.6
		6.5	12.0			180-195	27.5 ± 1	445	35	130	2.7	5
		7	13.0			190-210	28 ± 1	450	38	140	2.7	4.4
		8	14.0			210-225	28 ± 1	456	38	150	2.7	4
		9	15.5			225 \pm 5	28 ± 1	461	41	160	2.7	3.5

**Fig. 6** A typical microstructure of coaxial dendrite and reheat refine region at different locations of dissimilar SMA weld joint

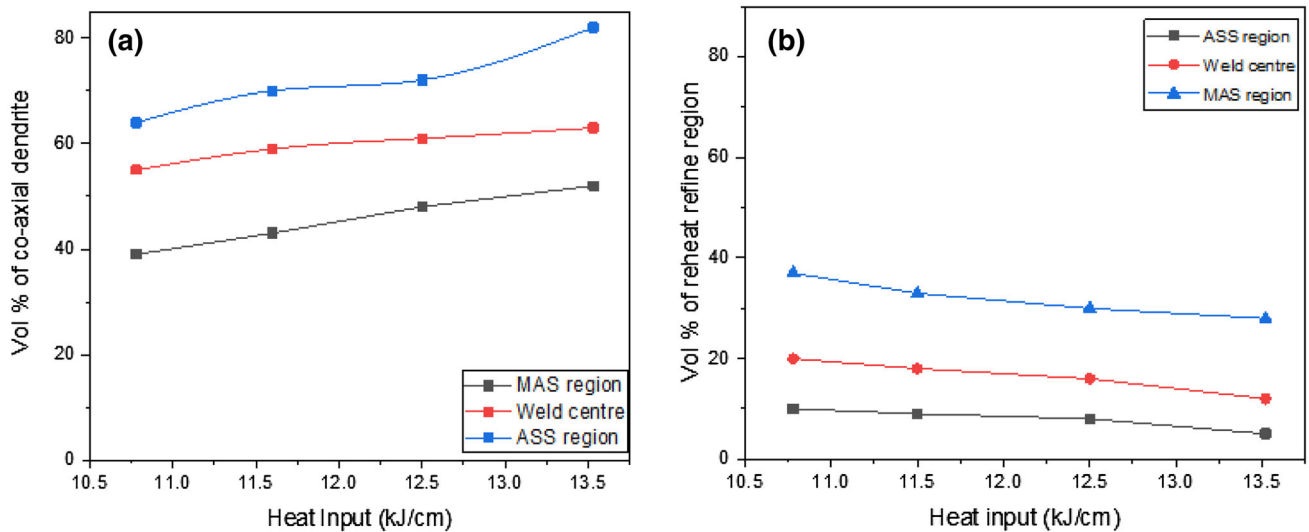


Fig. 7 Measured **a** coaxial dendrite and **b** rehear refine region at various locations of SMA weld of dissimilar ASS and MAS at different heat inputs

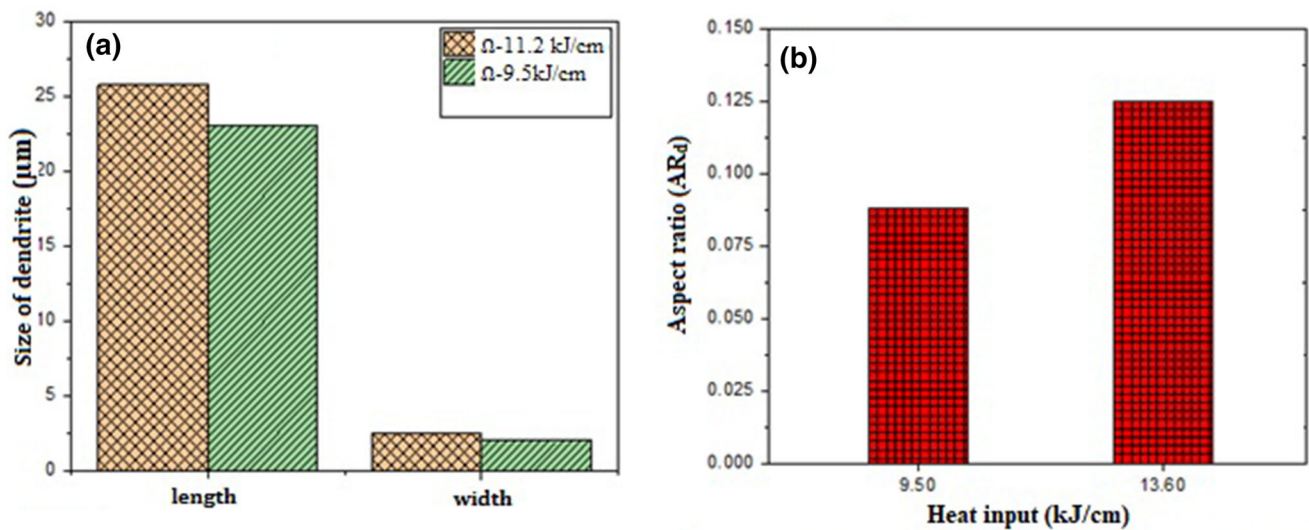


Fig. 8 The dendrite morphology of dissimilar SMA weld of ASS and MAS: **a** size of dendrite and **b** aspect ratio of different heat inputs of 11.2 ± 0.24 and 9.5 ± 0.42 kJ/cm

pool solidification [8, 17]. The solidification behavior of the weld metal influences to regulate the thermal behavior of the welding process, particularly in reference to the critical durations of the maximum temperature and the temperature above the formation of the grain growth with a better orientation of the dendritic growth of the grain structure. The heat and mass transfer are the important parameters for the development of the dendrite structure in the region of the transient condition during solidification [17–22]. The PGMAW process is preferred for its advantages such as a controlled weld thermal cycle and lower heat buildup in weld metal compared to the traditional GMAW process [23]. Hence, the PGMAW is a less heat

input process [24, 25], and it minimizes the residual stresses and favorably disturbs the weld metal mixture and phase change in the weld metal joint [26, 27]. The PGMAW process reduces the residual stresses of the weld joint because of its less heat input process.

However, the merits and success of the PGMA welding process are mainly reliant on the right choice of pulse factors, such as mean current (I_m), peak current (I_b), pulse duration (t_p), and pulse frequency (f). The pulse factor affects the weld metal microstructure, HAZ, weld chemistry, and amount of porosity in the weld owing to the effect on the thermal cycle of the weld metal and arc characteristics [28].

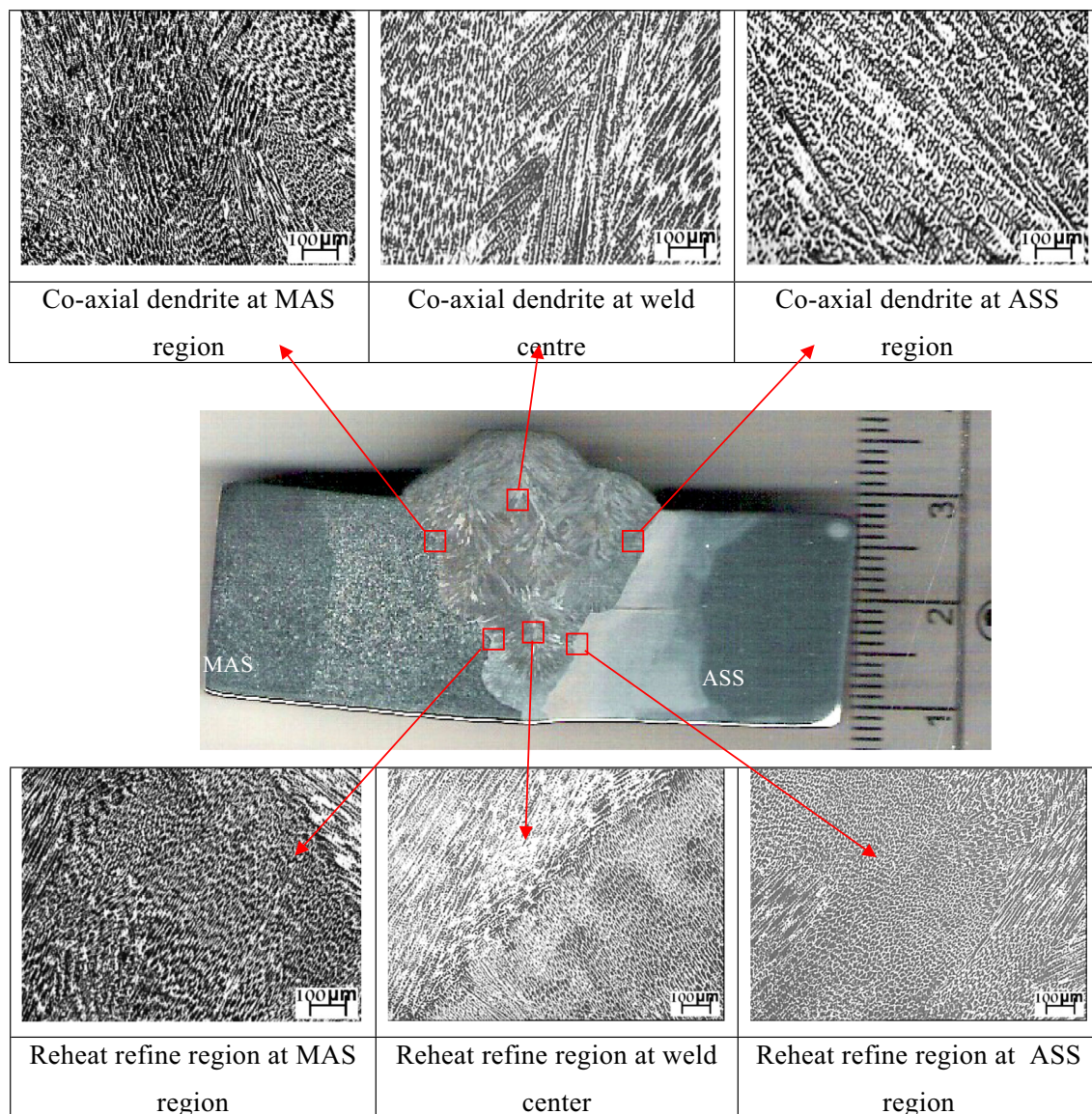


Fig. 9 Microstructure of coaxial dendrite and reheat refine at different regions of GMA weld of dissimilar ASS and MAS

The selection of pulse factors can be largely explained by using a brief effect of pulse factors that have been explained by a hypothetically developed dimensionless factor $\Phi = [(I_b/I_p) f t_b]$, where t_b is expressed as $[(1/f) - t_p]$ [29], which has been amply justified by several investigators in applications of pulsed current GMA welding on various materials [30–32]. After the literature survey, it was learned that the study on the dendrite morphology of the ASS and MAS dissimilar weld using the PGMA welding process was yet to be explored. Therefore, the present investigation pertains to studying the efficient use of factors ϕ , I_m , and Ω by analyzing their influence on thermal behavior, surface appearance, and dendrite morphology of weld deposition. The selection of an appropriate range of welding parameters and procedure, which may

effectively be used in pulse current gas metal arc welding of dissimilar austenitic stainless steel and micro-alloyed steel. This joint is highly promising for the application in nuclear power plants and in further studies about the influence of welding parameters on the dendrite morphology of the same welded metal samples.

2 Experimental Details

2.1 Base Metal and Welding Consumables

Base materials used for the current investigations were 20-mm-thick austenitic stainless steel plate of AISI 304LN grade and 20-mm controlled rolled plate of MAS-grade

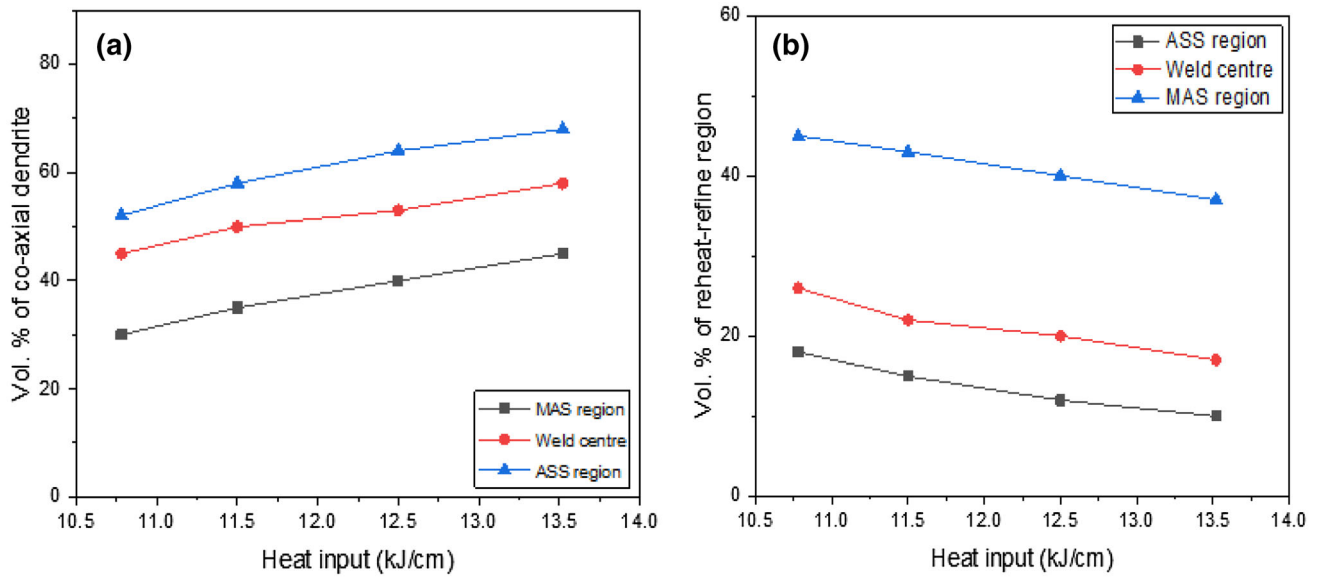


Fig. 10 At different heat inputs, the measurement of **a** coaxial dendrite and **b** reheat refine region at various locations in GMA weld of dissimilar ASS and MAS

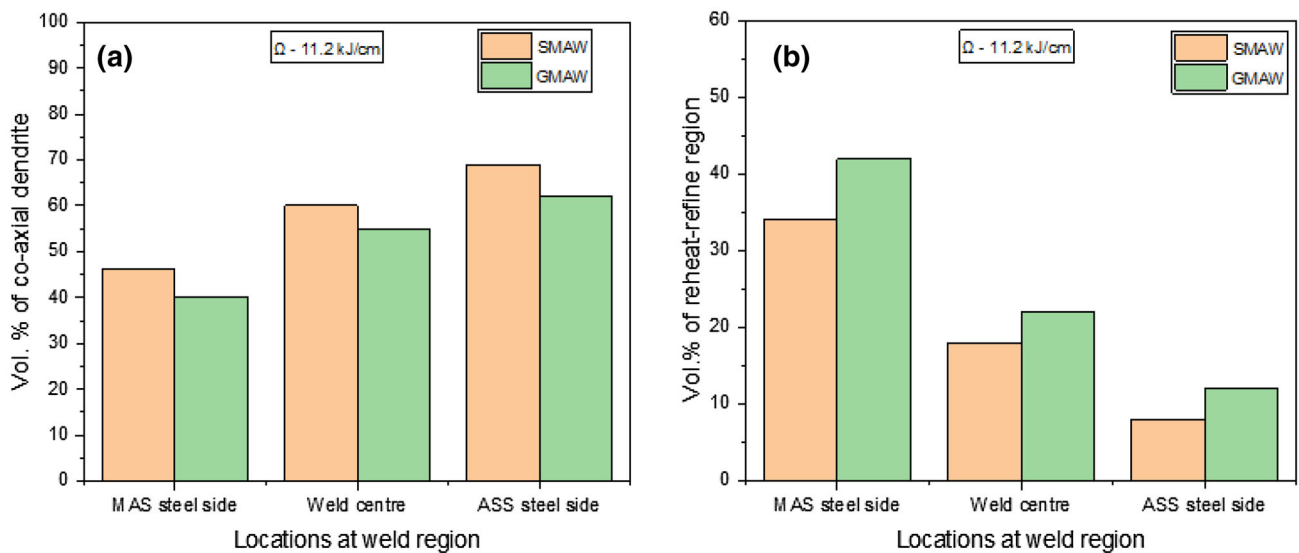


Fig. 11 At a given Ω (11.2 kJ/cm), the measurement of **a** coaxial dendrite and **b** reheat refine region at various locations in GMA and SMA weld of dissimilar ASS and MAS

SAILMA-350HI/SA533. The typical microstructure of transverse and longitudinal directions of the ASS and micro-alloyed steel base metal is shown in Figs. 1 and 2, respectively. Two different types of consumables were used in this experimentation, which included 1.2-mm-diameter stainless-steel filler wire (SFA-5.9 ER308L) in the GMA welding process and basic flux-coated 3.15-mm stainless-steel stick electrode (SFA-5.4 E308L-15) in the SMA welding process. Commercial argon of 99.98% purity was used as shielding gas in GMA and PGMA welding

processes with bare filler wire. Chemical compositions of the base metal (ASS and MAS) and welding consumables are detailed in Table 1.

2.2 Welding Process

The conventional V-groove (included angle of 60°–75°) was prepared in accordance with AWS specification, and it is schematically shown in Fig. 3 [33]. Introspection of the groove was surface carried out visually followed by a dye

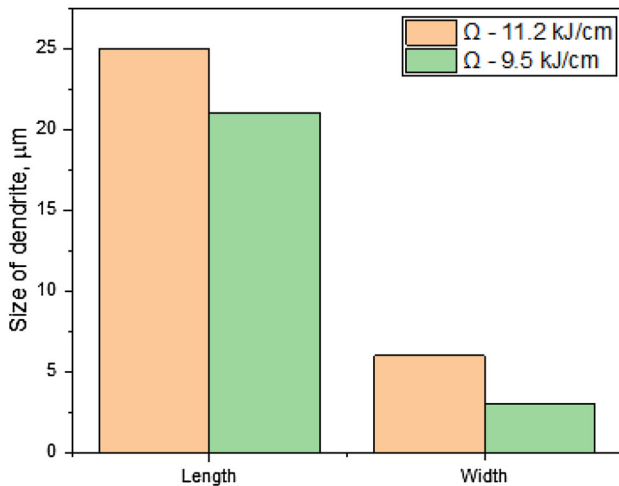


Fig. 12 The dendrite morphology of GMA weld of dissimilar ASS and MAS at different heat inputs of 11.2 ± 0.24 and 9.5 ± 0.42 kJ/cm

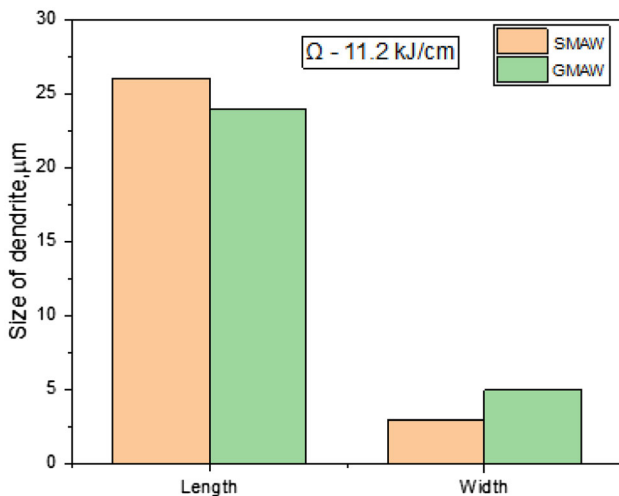


Fig. 13 At a constant Ω 11.2 kJ/cm, the variations in dendrite morphology (length and width) in GMA and SMA welds of dissimilar ASS and MAS

penetrant test to ensure the defect-free groove wall. The weld joints were prepared by one root pass of autogenous GTA welding, two filling pass of GTA, and subsequent filling passes by GMA and PGMA welding processes. Before welding, the 20-mm-thick high-strength low-alloy steel (MAS) plate of specification SAILMA-410HI/SA543 grade was preheated at about 125–130 °C for 60 s, and SMA welding electrodes were baked at 250 °C for 1 h prior to welding. The weld joints were prepared by using a direct current reverse polarity (DCRP). The welding was carried out without placing the root gap between the base

plates. A copper backing plate was used to support the base plates inadequate with a mild-steel plate support. The arrangement of the fixture is shown in Fig. 4.

The base plates were cleaned properly to remove grease, dirt, and oil contaminants sticking to the faying surface. The photograph of the experimental setup used for welding is shown in Fig. 5. Further, Table 2 shows the selection of different welding parameters used for making the dissimilar weld joints in various welding processes and procedures.

2.3 Dendrite Morphological Study

Weld deposition of the dissimilar welded samples was subjected to microstructural analysis in order to pursue a qualitative understanding about the grain size, and it was accomplished using optical microscope Axiovert 200 MAT and scanning electron microscope (model 435VF of M/s LEO Electron Microscopy Limited). Micro-pictures were mainly focused at the central part of the weld, particularly avoiding its narrow region near to the fusion zone. In particular, SEM images were analyzed by capturing 20 images at the molten zone at suitable magnification (100X–800X) to reveal the dendrite features.

Area fraction of the coaxial dendrite and reheat refined regions present in the three locations of the matrix as weld metal adjacent to the MAS steel region, weld center, and weld metal adjacent to the ASS region of the dissimilar SMA, GMA and PGMAW welds was measured using optical microscope by introducing a standard linear intercept method [34, 35].

The quantitative analysis of the primary dendrite morphology of the weld metal was defined by its length (L_d) and width (W_d). The captured images in the computer were analyzed by using Adobe Photoshop 7.0 software. The correctness of the images was also clarified by analyzing the images in the SEM microscope at suitable magnifications. The width of a dendrite (W_d) was calculated at different locations along the length of the dendrite (L_d), and the moderation of the entire readings was used to estimate the aspect ratio (AR_d) of the dendrites as follows:

$$AR_d = W_d/L_d \quad (2.1)$$

The average of all the measured values of the length and width of dendrites acquired from all the images of microstructure obtained from different specimens prepared at a given welding parameter was reported as a general characteristic of the weld deposit at respective locations.

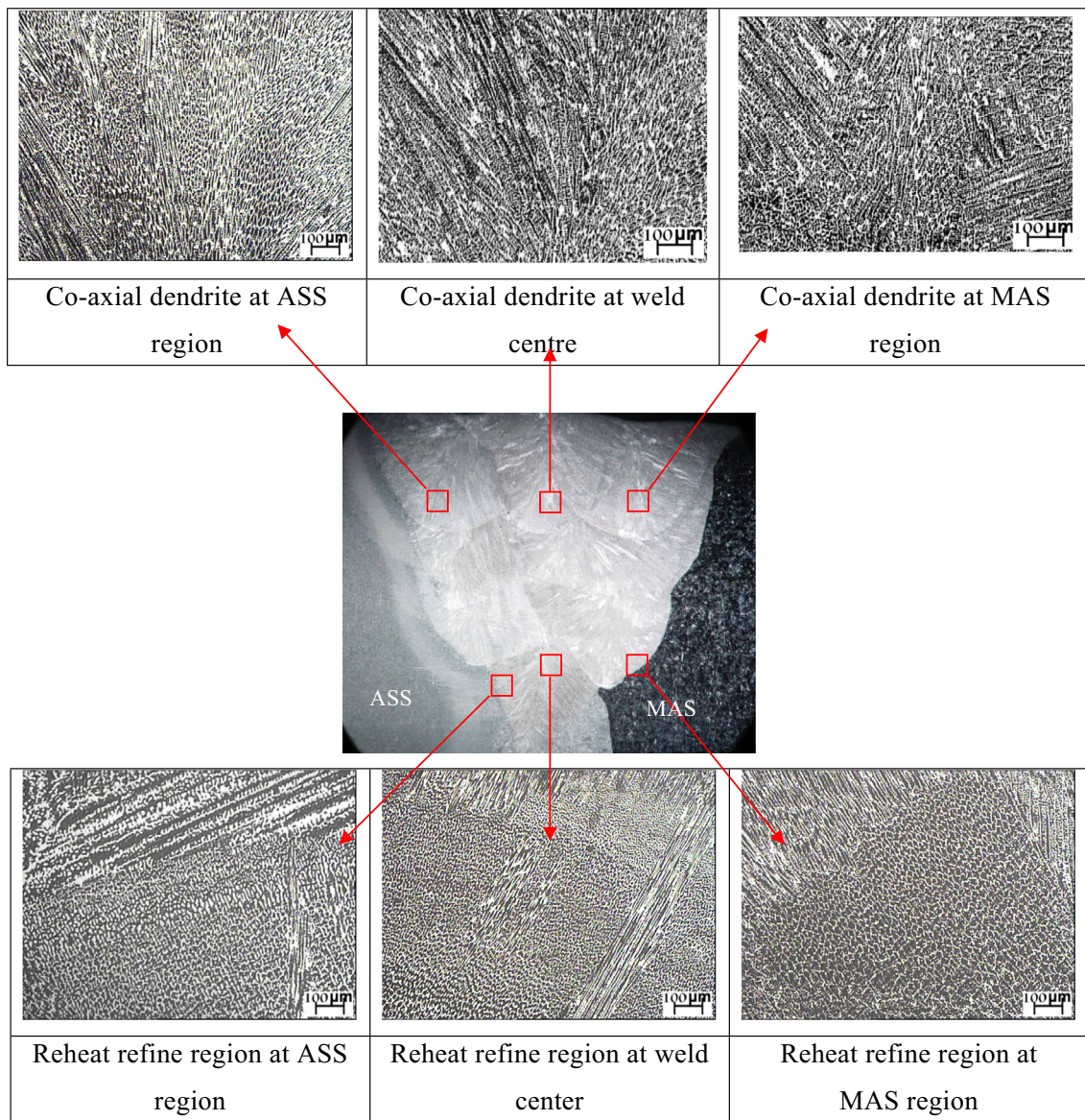


Fig. 14 A typical microstructure of coaxial dendrite and reheat refine region at different regions in PGMA weld of dissimilar ASS and MAS

3 Results and Discussion

3.1 Coaxial Dendrite on Dissimilar SMA Weld

The typical microstructure of coaxial dendrites and the reheat refine region at different locations of dissimilar SMA weld of ASS and MAS is shown in Fig. 6. The variation in coaxial dendrites and the reheat refine region at various locations during SMA welding processes is shown in Fig. 7a, b, respectively. It is evident from Fig. 7a that the increase in heat input increases the coaxial dendrite content irrespective of the regions; this may primarily occur owing to an increase in heat input. However, interestingly the slower heat dissipation in the ASS region enhances the dendrite formation, whereas in the case of

MAS region, it follows the converse because of the difference in the properties of thermal conductivity. In other words, heat dissipation on the MAS region occurs faster than on the ASS region, which comparatively leads to less formation of the coaxial dendrite. As far as weld center region is concerned, the formation of the coaxial dendrite is found to be quite higher than the ASS region which can be attributed to the slower heat dissipation.

Figure 7b shows that the increase in heat input drastically reduces the reheat refine region in all the locations, but after reaching the heat input of 12.5 kJ/cm, the change in the reheat refinement almost remains linear in all the regions because the higher Ω enhances the weld metal deposit, which leads to increase in the coaxial dendrite content and reduces the reheat refine region.

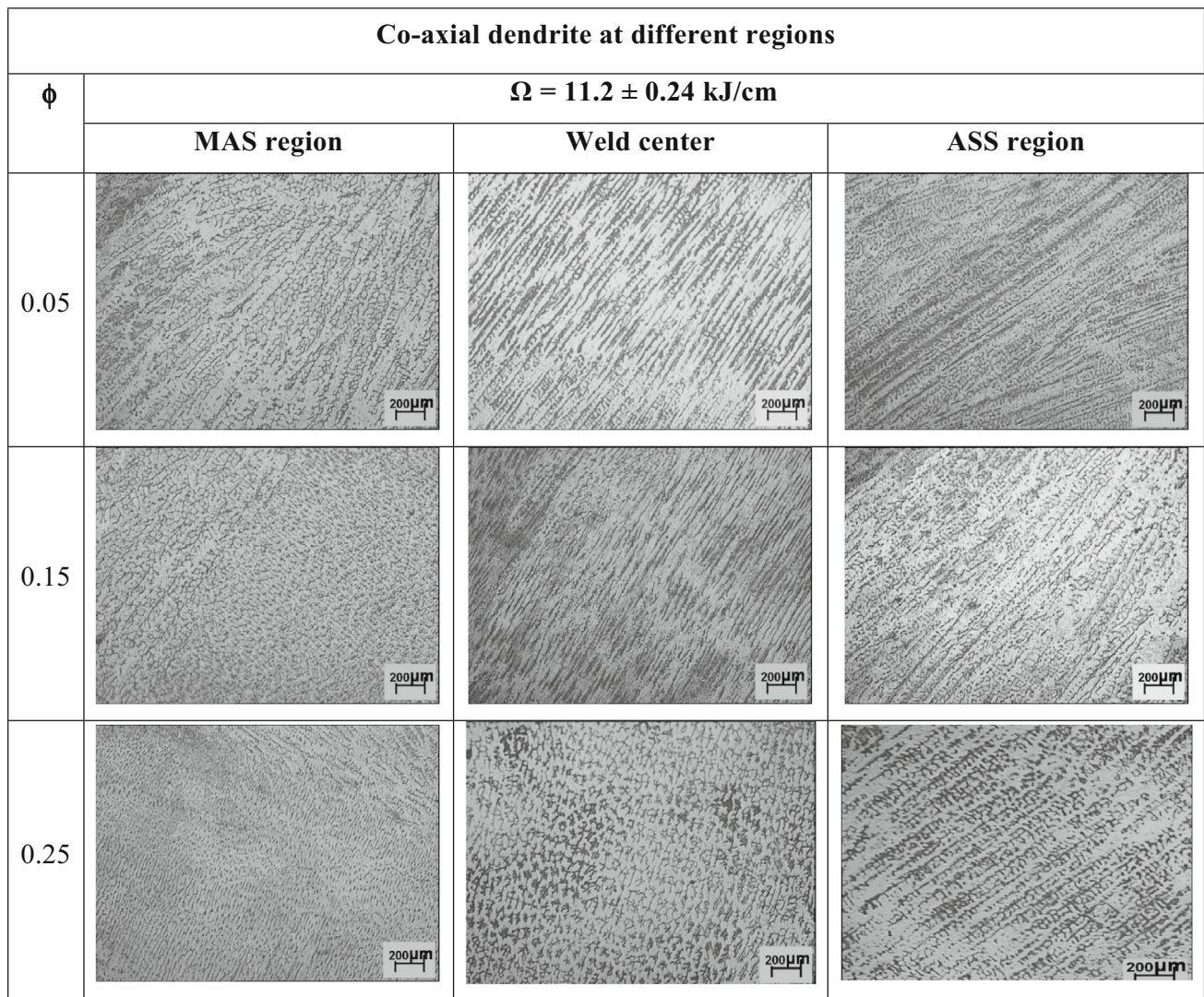


Fig. 15 At a given Ω (11.2 kJ/cm) and varying ϕ of 0.05, 0.15 and 0.25, the typical microstructure of coaxial dendrite at different regions in PGMA weld of dissimilar ASS and MAS

At a given higher and lower Ω of 11.2 and 9.5 kJ/cm, the variations in dendrite morphology in terms of size and aspect ratio of dissimilar SMA weld are shown in Fig. 8a, b, respectively. Graph plot reveals that the increase in heat input drastically enhances the dendrite length and width in all the locations; moreover, the higher Ω enhances the temperature of weld bead in multi-pass deposition and eventually reduces its cooling rate. In both the graphs, it is interesting to note that the thermal conductivity of the MAS is higher than that of ASS steel; hence, the dissipation of heat is very quick and it reduces the dimension of the dendrite length and width.

3.2 Coaxial Dendrite on GMA Dissimilar Weld

The variation in the macrostructure of coaxial dendrites and reheat refine region at different locations in GMA dissimilar weld joint of ASS and MAS is shown in Fig. 9. From Fig. 10a, b, it is observed that the increase in Ω moderately enhances the volume of coaxial dendrite content and significantly reduces the volume of reheat refine region in all the locations. The volume of dendrite and the volume of reheat refine region have been estimated at a constant Ω value of 11.2 kJ/cm. From Fig. 11a, b, it is evident that SMA weld shows a higher volume percentage of coaxial dendrite and a lower volume percentage of reheat refine region in MAS and ASS regions, respectively. In the case of the GMA welding process, the weld center

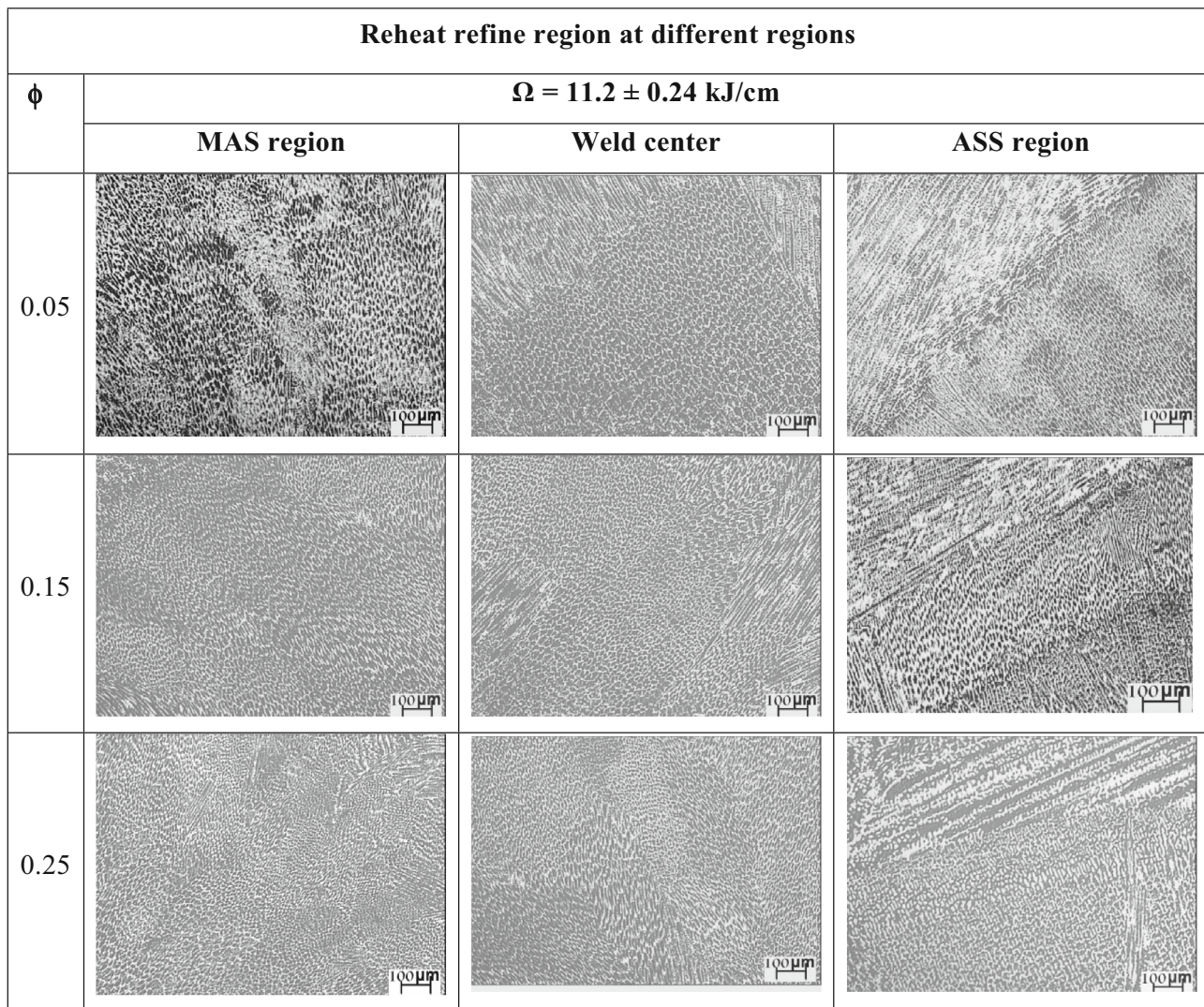


Fig. 16 At a given Ω (11.2 kJ/cm) and varying ϕ of 0.05, 0.15 and 0.25, the typical microstructure of reheat refine region at different regions in PGMA weld of dissimilar ASS and MAS

and ASS region exhibit a higher volume percentage of coaxial dendrite and a lower volume percentage of reheat refine region, whereas the MAS region follows another way around. This effect is due to the severity of the thermal cycle from the multi-pass weld of the GMAW process.

The variations in coaxial dendrite morphology (length and width) in the GMA weld joint of dissimilar ASS and MAS at a given higher and lower Ω with values 11.2 and 9.5 kJ/cm respectively are shown in Fig. 12. From the graph plot, it is observed that the increase in heat input drastically enhances the coaxial dendrite length and width in the entire region of the weld. The comparative analysis of variations in coaxial dendrite morphology (length and width) in GMA and SMA weld joint of dissimilar ASS and MAS at a given Ω (11.2 kJ/cm) is exhibited in Fig. 13. It

can be noticed that the length of coaxial dendrite is relatively reduced and the width of dendrite comparatively enhances the dissimilar GMA weld than SMA weld. It may happen due to the nature of GMAW metal transfer and the severity of the weld thermal cycle.

3.3 Coaxial Dendrite on Dissimilar PGMA Weld

The typical macrostructure of coaxial dendrites and reheat refine region at different locations of PGMA weld joint of dissimilar metals of ASS and MAS is typically shown in Fig. 14. At a constant heat input (Ω) of 11.2 kJ/cm, the influence of ϕ on variations in the microstructure of coaxial dendrites and reheat refine region at different locations of dissimilar weld joint prepared by using the PGMA welding

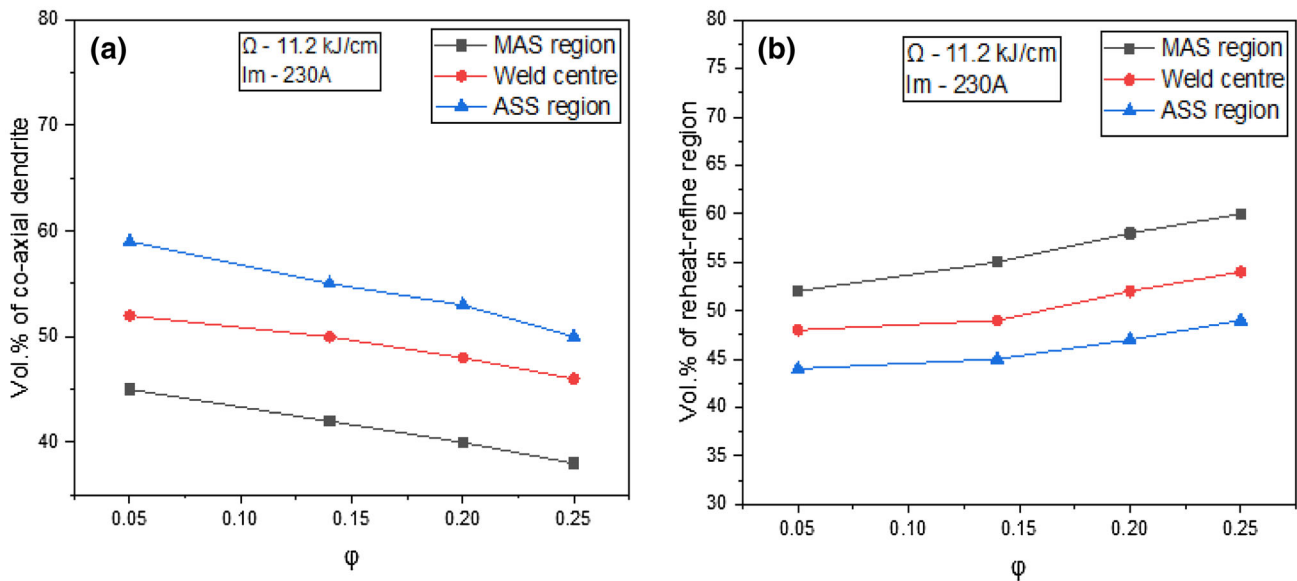


Fig. 17 The measurement of **a** coaxial dendrite and **b** reheat refine region at various locations in PGMA weld of dissimilar ASS and MAS at given Ω (11.2 kJ/cm), I_m (230 A), and varying ϕ

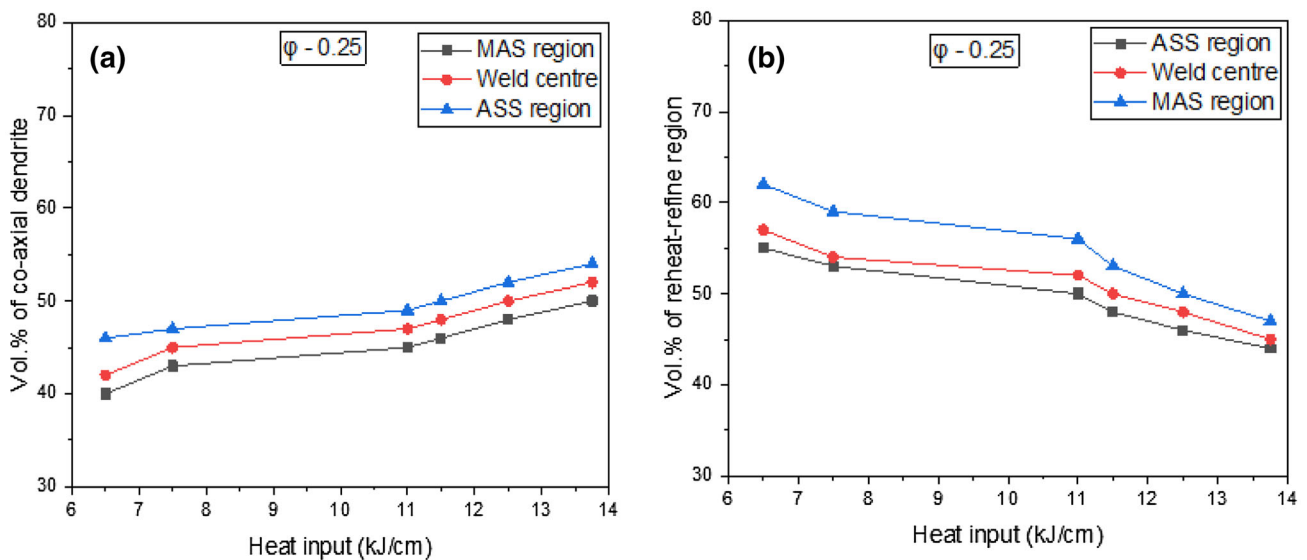


Fig. 18 The measurement of **a** coaxial dendrite and **b** reheat refine region at various locations in PGMA weld of dissimilar ASS and MAS at given ϕ of 0.25 and varying heat inputs

process is displayed in Figs. 15 and 16, respectively. The figure clearly tells all about an increase in heat input (Ω) and moderate enhancement of the coaxial dendrite content in all the regions. The higher heat input (Ω) significantly enhances the temperature of the bead, and this high-temperature bead further increases the width of HAZ. If the HAZ width is larger, then the heat dissipation from the weld metal to the MAS base metal is reduced. So, due to the slower heat dissipation, the dendrite formation is enhanced in the ASS region, but in the case of the MAS region, its thermal conductivity is comparatively greater

than the ASS base metal. Therefore, heat dissipation is faster in the MAS region; hence, dendrite formation reduces substantially. In the weld center, the heat dissipation again reduces due to the distance of the sink from the weld center. So, due to a lower heat dissipation, the dendrite formation is more in the weld center but in comparison with the ASS region, the coaxial dendrite percentage is lower in the weld center region.

At a given heat input Ω (11.2 kJ/cm), the measured coaxial dendrite and reheat refine regions at different locations of the weld are displayed in Fig. 17a, b. The

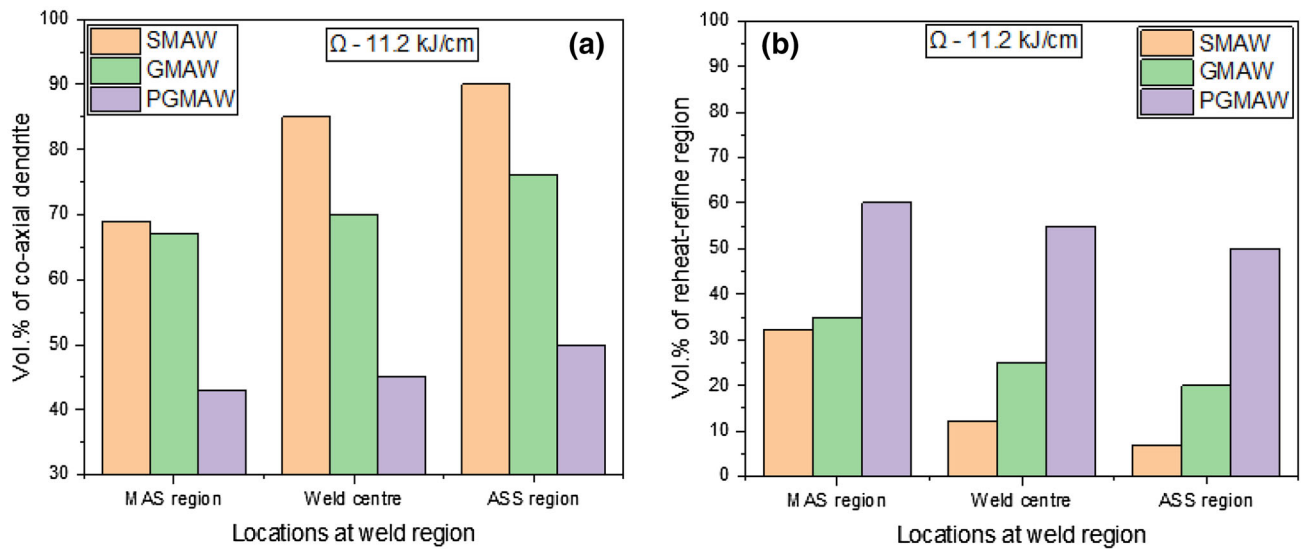


Fig. 19 At a given Ω (11.2 kJ/cm), the comparative analysis of **a** coaxial dendrite and **b** reheat refine region at various locations in PGMA, GMA and SMA weld of dissimilar ASS and MAS

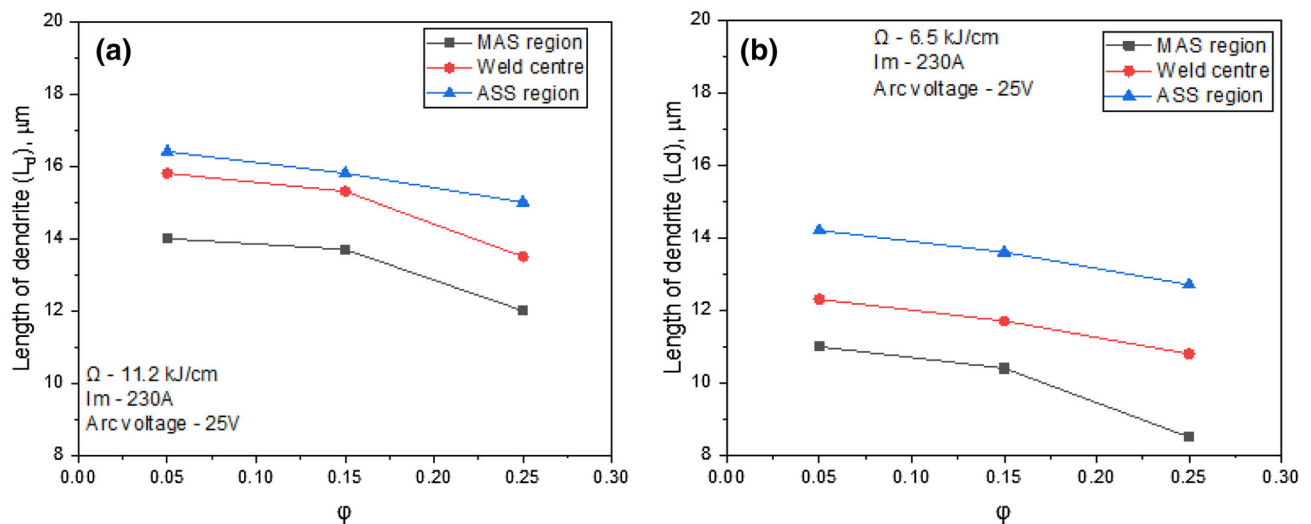


Fig. 20 At a given I_m (203A), arc voltage (25 ± 1 V), and varying ϕ of 0.05, 0.15 and 0.25, respectively, the length of dendrite at different Ω **a** 11.2 ± 0.24 and **b** 6.5 ± 0.42 kJ/cm

figure shows that the increase in ϕ relatively decreases the coaxial dendrite percentage and consequently enhances the reheat refine region in all the specified locations of the weld. This may be because at a given arc voltage and ϕ , the arc heat that is transferred to the weld pool (Q_{AW}) and heat of the filler metal, that is transferred to the weld pool (Q_f) are enhanced with the increase in I_m . However, the figure also shows that at a given I_m and arc voltage the Q_{AW} and Q_f reduce marginally with the increase in ϕ from 0.05 to 0.25. This may have primarily happened because

the heat content per unit mass of droplet (Q_{de}) and temperature of the droplet (T_{de}) considerably reduce with the increase in ϕ . This may be because the increase in ϕ decreases the QT and enhances the cooling rate significantly making the reheat refine region as explained earlier [32, 33]. At a given ϕ (0.25), the effect of heat input (Ω) on the volume of coaxial dendrite and reheat refine region at various locations of the dissimilar PGMA weld is shown in Fig. 18a, b. The figures express that the increase in heat input (Ω) marginally enhances the coaxial dendrite content

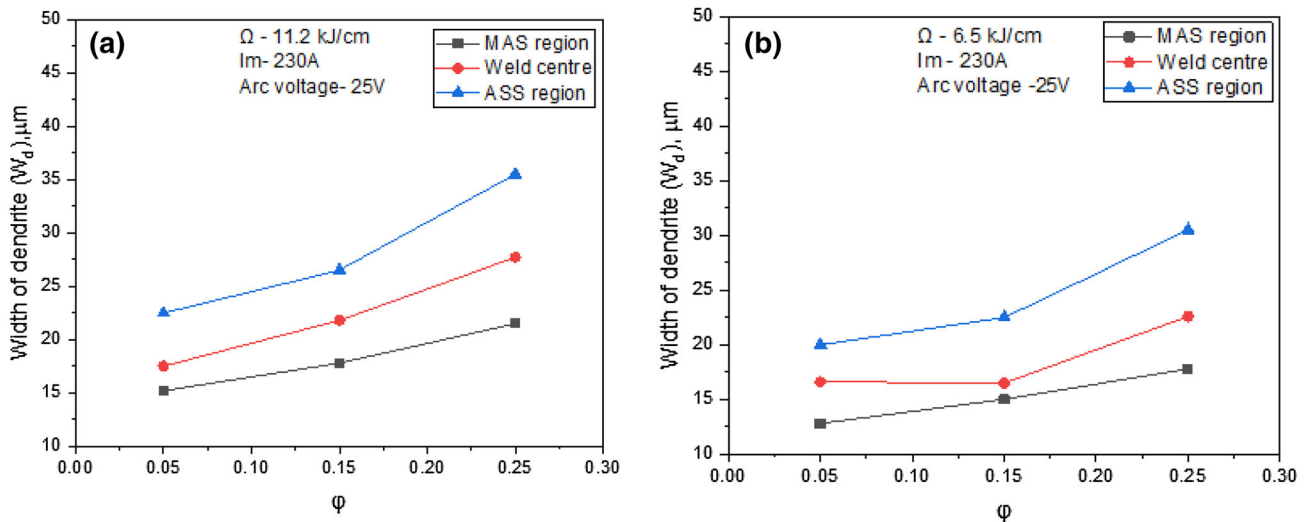


Fig. 21 At a given I_m (230A), arc voltage (25 ± 1 V), and varying ϕ of 0.05, 0.15 and 0.25, respectively, the width of dendrite at different Ω a 11.2 ± 0.24 and b 6.5 ± 0.42 kJ/cm

of all the regions, but after reaching the Ω of 12.5 kJ/cm the changes in coaxial dendrite formation are almost linear in all the regions because the higher Ω enhances the weld metal deposit; if the weld metal deposit increases, then the remelting of the previous bead also increases, which enhances the reheat refine region.

The estimated dendrite and reheat refine regions in the dissimilar weld of ASS and MAS metals using PGMA, GMA, and SMA weld are shown in Fig. 19a, b. It is mainly observed that dissimilar PGMA weld has a comparatively higher volume percentage of reheat refine region and a lower coaxial dendrite than the GMA and SMA dissimilar weld. This may be attributed to the discontinuity of the metal deposition in the PGMA welding process imparted by the pulse effect. The thermal shock during solidification is through the typical reheat refinement microstructure by the following weld bead, and moreover, the quantity of heat transferred to the weld pool (QT) is reduced by the increase in ϕ , which has been discussed earlier.

The morphology of coaxial dendrite can be understood by its length and width. At a given I_m of 230A, by varying ϕ to 0.05, 0.15, and 0.25, the length of primary growth of dendrite at relatively higher and lower Ω of 11.2 and 6.5 kJ/cm, respectively, is displayed in Fig. 20a, b. Under the same conditions, the effect of ϕ on the width of primary dendrite at the above-mentioned higher and lower Ω is shown in Fig. 21a, b, respectively.

The figures express that at constant Ω the increase in ϕ reduces the length of dendrite but increases its width

significantly in all concerned locations of the weld. This mainly occurs because the increase in ϕ reduces the quantity of heat transfer to the weld (QT). It also represents that the increase in Ω at given ϕ appreciably enhances the length and width of dendrite in all the locations because the higher Ω enhances the temperature of weld bead in multi-pass deposition reducing its cooling rate.

Figure 22 shows the dendrite morphological behavior of the weld in a different location at a given Ω of 11.2 kJ/cm with varying ϕ . The increase in Ω moderately enhances the dendrite length and width in all the locations of weld. The higher Ω produces higher temperature of weld bead with wider width of HAZ. The wider HAZ delays heat dissipation from the weld metal to the base metal enhancing the length and width of dendrite. The thermal conductivity of micro-alloyed steel is comparatively higher than ASS base metal; thus, at a given Ω the heat dissipation is relatively faster in micro-alloyed steel side, and it reduces the length of dendrite. At weld center, the heat dissipation is again reduced due to its longer distance from sink, which lowers the heat dissipation relatively enhancing the length of dendrite in comparison with that of the micro-alloyed steel side of the weld. However, in this situation the heat dissipation possibly becomes slowest in the location of the weld adjacent to the low thermal conductive γ -SS base metal causing maximum coarsening of the morphology of primary dendrites.

At a given heat input (Ω) of 6.5 kJ/cm, a significant variation is found in the dendrite morphology (Fig. 23) in

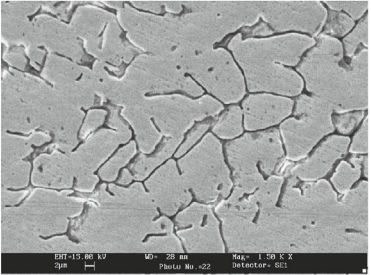
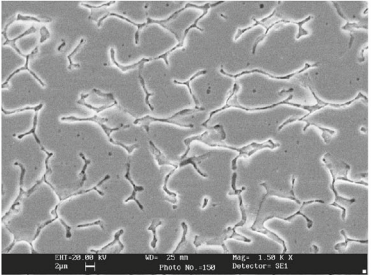
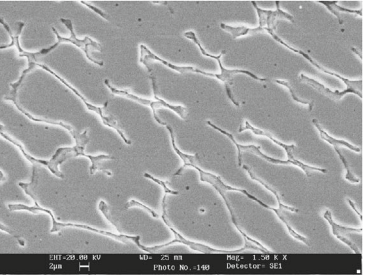
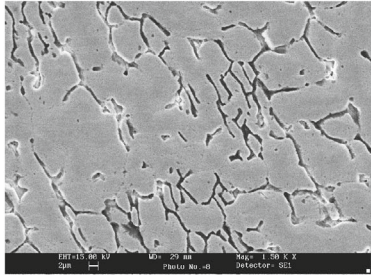
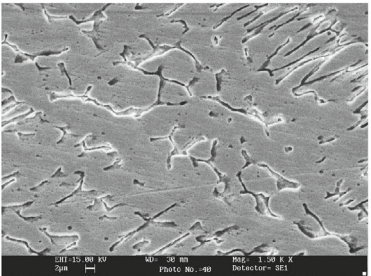
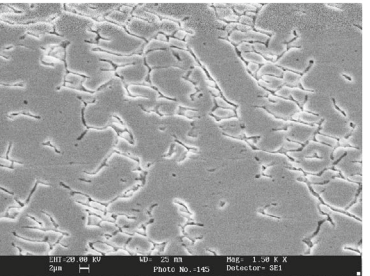
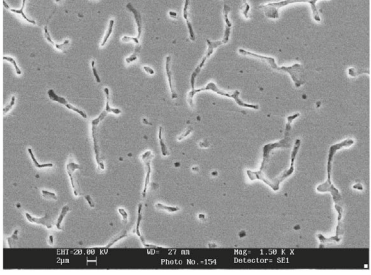
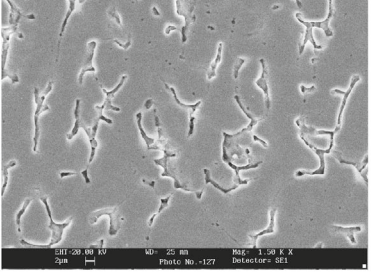
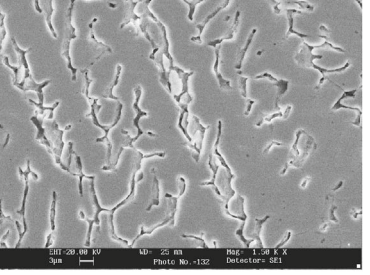
Dendrite morphology at different regions			
ϕ	$\Omega = 11.2 \pm 0.24 \text{ kJ/cm}$		
	MAS region	Weld center	ASS region
0.05			
0.15			
0.25			

Fig. 22 At a given Ω (6.5 kJ/cm) and varying ϕ , typical dendrite morphology of dissimilar weld joint at different regions

all the locations of PGMA, GMA, and SMA weld. It is primarily observed from the figure that the dissimilar PGMA weld joint has a comparatively shorter length and width of dendrite than the GMAW and SMAW. In the PGMAW process, the quantity of heat that is transferred to the weld pool (QT) is relatively lower than the GMAW and SMAW processes. The variations of (ϕ) and (QT) are primarily influenced in dendrite morphological dimensions.

4 Conclusion

The comparative analysis pertaining to dendrite morphological behavior of dissimilar welded metals using SMA, GMA, and PGMA was studied, and following inferences were drawn:

- At a constant Ω and I_m , the dissimilar PGMA weld deposit adjacent to MAS base plate was found to have comparatively more amount of reheat refine region than the weld deposit existing adjacent to the ASS base plate with the increase in ϕ .
- At a given Ω , the weld deposit adjacent to the ASS and MAS base metals in PGMA weld was found to have a comparatively lower coaxial dendrite content than GMA and SMA welds.
- The dissimilar PGMA welds had more amount of refined dendritic microstructure, especially with the lowering of ϕ than GMA and SMA welds (similar Ω).
- At a given Ω and I_m , the dissimilar PGMA with the increase in ϕ significantly reduced the grain size near to the fusion zone in the ASS region than in the MAS region.

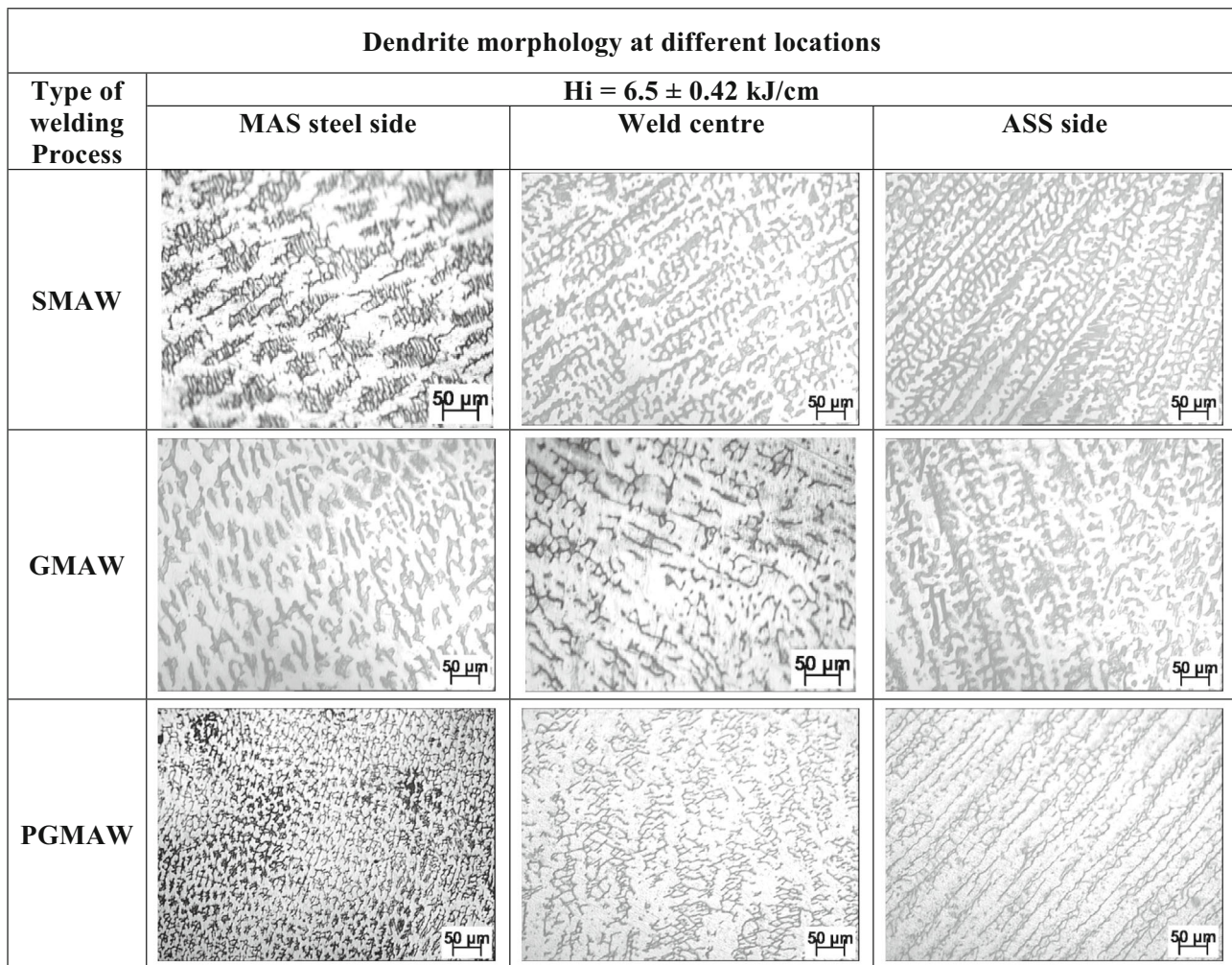


Fig. 23 At a given Ω (6.5 kJ/cm), typical variation in dendrite morphology at different locations of dissimilar PGMA, GMA, and SMA weld joints

- In comparison with GMAW and SMAW, the PGMAW process could produce sound weld at relatively lower Ω of 9.2 + 0.3 kJ/cm with a low ϕ of 0.05.
- The PGMAW process enhanced the microstructure of refined grains in multiple layers of weld, and this phenomenon was found obviously in the MAS and ASS steel regions. It was also identified that the PGMAW process was suitable for the dissimilar weld when compared to GMAW and SMAW processes.

Acknowledgments The authors thankfully acknowledge the Board of Research in Nuclear Sciences (BRNS) for the material support to carry out this work.

References

1. Yufeng S, Sili F, and Changwei X, *Res Phys* **11** (2018) 853.
2. Huang M L, and Wang L, *Metall Mat Trans A* **29A** (1982) 3037.
3. Marshall W, *An assessment of integrity of PWR pressure vessels, second report by a study group under the chairmanship of, United Kingdom Atomic Energy Authority*, 14 (1982) (Section-5).
4. Singh D K, Sahoo G, Basu R, Sharma V, and Mohtadi-Bonab M A, *J Manuf Process* **36** (2018) 281.
5. Rajamurugan G, Dinesh D, and Ramakrishnan A, *Int J Mech Prod Eng Res Dev* **8** (2018) 1641.
6. Lundin C D, *Weld Res Suppl* **61** (1982) 58.
7. Faber G, and Gooch T, *Weld World* **20** (1982) 88.
8. Castro R J, and de Cadenet J, *Welding Metallurgy of stainless steel and Heat-Resisting Steel*, Cambridge University Press, Cambridge (1974) p 158.
9. Gauzzi F, and Missori S, *J Mater Sci* **23** (1988) 782.
10. Sadeghian M, Shamanian M, and Shafyei A, *Mater Des* **60** (2014) 678.
11. Hajiannia I, Shamanian M, and Kasiri M, *Mater Des* **50** (2013) 566.
12. Cam G, Yeni C, Erim S, Ventzke V, and Kocak M, *SciTechnol Weld Joint* **3** (1998) 177.
13. Rossini M, Spena P R, Cortese L, Matteis P, and Firrao D, *Mater Sci Eng A* **628** (2015) 288.
14. Hernandez B V H, Kuntz M L, Khan M I, and Zhou Y, *SciTechnol Weld Join* **13** (2008) 769.

15. Pouranvari M, Mousavizadeh S M, Marashi S P H, Goodarzi M, and Ghorbani M, *Mater Des* **32** (2011) 1390.
16. American Welding Society, *Metals and Their Weldability. Welding Handbook, Section IV* (1972) 67.37.
17. David S A, and Vitek J M, *Int Mater Rev* **34** (1989) 213.
18. Kou S, Sun D, *Metall Mater Trans A* **16** (1985) 203.
19. Arora A, Roy G G, DebRoy T, *Scr Mater* **60** (2009) 68.
20. Lienert T J, Burgardt P, Harada K L, Forsyth R T, and DebRoy T, *Scr Mater* **71** (2014) 37.
21. Mishra S, Lienert T, Johnson M, DebRoy T, *ActaMater* **56** (2008) 2133.
22. Lu S P, Fujii H, and Nogi K, *Scr Mater* **51** (2004) 271.
23. Ghosh P K, Goyal V K, Dhiman H K, and Kumar M, *Sci Technol Weld Join* **11** (2006) 232.
24. Ferraresi V A, Figueiredo K M, Ong H T, *J Brazilian Soc Mech Sci Engg* **XXV** (2003) 229.
25. Joseph A, Harwig D, Farson D F, and Richardson R, *Sci Technol Weld Join* **8** (2003) 400.
26. Zhang Y M, Liguó E, and Kovacevic R, *Weld J* (1998) 458s.
27. Gupta P C, Ghosh P K, and Vissa S, *Int Conf Weld Technol UOR* (1998) 171.
28. Ghosh P K, and Sharma V, *Mater Trans JIM* **32** (1991) 145.
29. Ghosh P K, Gupta P C, Ghosh P K, Gupta S R, and Jain N K, *Indian Weld J* (1989) 550.
30. Ghosh P K, and Dorn L, *Int J Join Mater* **5** (1993) 143.
31. Ghosh P K, *Int J Join Mater* **8** (1996) 157.
32. Rajamurugan G, Dinesh D, and Ramakrishnan A, *Int J Mech Prod Eng Res Dev* **8** (2018) 1641. Rajamurugan G, and Ghosh P K, *Asian J Res Soc Sci Human* **6** (2016) 267. <https://doi.org/10.5958/2249-7315.2016.00395.6>.
33. American Welding Society, *Welding Handbook, Section IV, Sixth Edition* (1972) p 67.37.
34. Goyal V K, Ghosh P K, and Saini J S, *Metall Mater Trans A* **38** (2007) 1794.
35. Rajamurugan G, and Ghosh P K, *Asian J Res Soc Sci Human* **6** (2016) 277. <https://doi.org/10.5958/2249-7315.2016.00396.8>.

Publisher's Note Springer Nature remains neutral with regard to jurisdictional claims in published maps and institutional affiliations.